Received 12 October 2022; revised 2 December 2022 and 12 December 2022; accepted 14 December 2022. Date of publication 20 December 2022; date of current version 21 February 2023. The review of this article was arranged by Editor M. Saitoh.

Digital Object Identifier 10.1109/JEDS.2022.3230402

Investigation of Recovery Phenomena in $Hf_{0.5}Zr_{0.5}O_2$-Based 1T1C FeRAM

JUN OKUNO [1] (Member, IEEE), TSUBASA YONAI [1], TAKAFUMI KUNIHIRO [1], YUSUKE SHUTO [1] (Member, IEEE), RUBEN ALCALA [2] (Graduate Student Member, IEEE), MAXIMILIAN LEDERER [3], KONRAD SEIDEL [3], THOMAS MIKOLAJICK [2,4] (Senior Member, IEEE), UWE SCHROEDER [2] (Senior Member, IEEE), MASANORI TSUKAMOTO [1], AND TAKU UMEBAYASHI [1]

1 Research Division 1, Sony Semiconductor Solutions Corporation, Atsugi 243-0014, Kanagawa, Japan
2 NaMLab gGmbH, 01187 Dresden, Germany
3 Fraunhofer IPMS-Center Nanoelectronics Technologies, 01099 Dresden, Germany
4 IHM, TU Dresden, 01062 Dresden, Germany

CORRESPONDING AUTHOR: J. OKUNO (e-mail: Jun.Okuno@sony.com)

ABSTRACT We have previously studied fatigue and its recovery phenomenon on 64 kbits hafnium-based one-transistor and one-capacitor (1T1C) ferroelectric random-access memory (FeRAM) with PVD-TiN (30 nm)/ALD- $Hf_{0.5}Zr_{0.5}O_2$ (8 nm)/CVD-TiN (50 nm) capacitors. In this study, we characterized a single large capacitor fabricated using the same process as the 1T1C FeRAM to clearly understand the recovery mechanism and comprehensively qualify the recovery effect. The results reveal that the recovery effect is caused by domain depinning and new domains switching owing to a redistribution of oxygen vacancy. Furthermore, it is evident from recovery voltage and recovery pulse width dependence of the recovery effect that the recovery voltage can be reduced by applying a longer recovery pulse width. This enables a more flexible circuit design of 1T1C FeRAM when the recovery method is applied to enhance the cycling endurance.

INDEX TERMS Capacitor, hafnium oxide, ferroelectric random-access memory, recovery, zirconium oxide.

I. INTRODUCTION

HfO_2-based ferroelectric devices have been increasingly discussed in recent years owing to good compatibility of cutting-edge CMOS logic process and lower switching current than other resistive random-access memories (RRAMs) [1], [2], [3]. Zr-doped HfO_2 (HZO) are widely discussed toward various ferroelectric random-access memory (FeRAM) applications [4], [5], [6], [7]. One-transistor one-capacitor (1T1C) FeRAM with metal/ferroelectric/metal (MFM) capacitors allows high cycling tolerance owing to its good interface between the ferroelectric layer and metal electrodes than metal/ferroelectric/silicon capacitors [8], [9], [10]. However, a degradation of remanent polarization during cycling stress called "fatigue" required to be concerned [11], [12], [13]. The mechanism of fatigue has been widely discussed and the increase in the trap density near the electrodes results in the domain pinning of dipoles. References [14], [15], [16], [17]. Furthermore, positively charged oxygen vacancies formed by electron de-trapping at the interface between HZO and electrodes can cause domain pinning, and the fatigue can be recovered by applying a high stress field [18], [19]. Previously, we have revealed that the fatigue and recovery phenomenon are caused by the uniform usage of 64-kbits of 1T1C FeRAM memory array with $Hf_{0.5}Zr_{0.5}O_2$-based capacitors under a fatigue stress condition of 2.0 V at 10 MHz and recovery stress condition of 2.8 V at 10 MHz [20]. In this paper, we have extended our prior work and performed a detailed analysis using a single large capacitor that was fabricated using a same process to 1T1C FeRAM to clearly understand the recovery mechanism and comprehensively investigate the recovery effect.

II. EXPERIMENT

A 64 kbits-1T1C FeRAM memory array and a large capacitor were simultaneously fabricated using the same process [11]. The large capacitor (total area of 1,000 μm^2) was prepared by connecting 1,000 capacitors of the same size and structure as the 1T1C FeRAM memory cell, which has an area

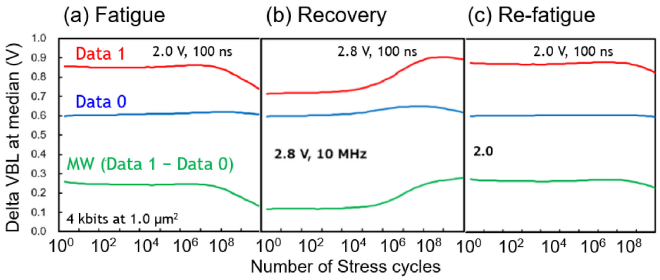

FIGURE 1. (a) Fatigue measurement result up to 10^{10} cycles with a cycling stress voltage of 2.0 V and the pulse width of 100 ns (b) Recovery test result of 10^{10} cycles with a cycling stress voltage of 2.8 V and the pulse width of 100 ns, and (c) Re-fatigue test results for 10^{10} cycles post recovery with a cycling stress voltage of 2.0 V and the pulse width of 100 ns. Median value of ΔV_{BL} (Bitline voltage shift of the 1T1C FeRAM) in 4 kbits MFM cells are extracted [20].

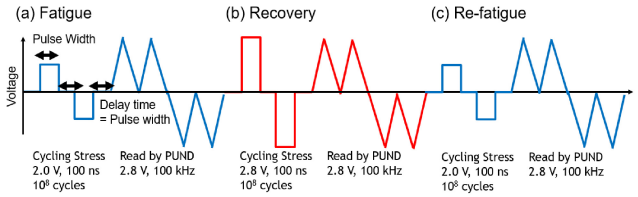

FIGURE 2. Measurement sequence during (a) Fatigue up to 10^8 cycles with a cycling stress voltage of 2.0 V and the pulse width of 100 ns (b) Recovery up to 10^8 cycles with a cycling stress voltage of 2.8 V and the pulse width of 100 ns, and (c) Re-fatigue up to 10^8 cycles with a cycling stress voltage of 2.0 V and the pulse width of 100 ns.

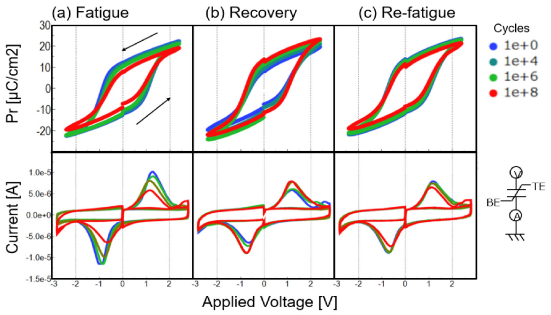

FIGURE 3. P-V curve and I-V curve obtained from PUND results during (a) Fatigue, (b) Recovery, and (c) Re-fatigue phases. Positive bias was applied from top electrodes. Voltage range of the P-V cure was limited to −2.4 V to 2.4 V to extract the 2·Pr.

of 1 μm^2 (length of 1.25 μm and width of 0.80 μm). PVD-TiN (30 nm)/ALD- $Hf_{0.5}Zr_{0.5}O_2$ (8 nm)/CVD-TiN (50 nm) were stacked as the MFM capacitor. For the capacitor, a positive-up-negative-down (PUND) of the fatigue and its recovery was conducted using an Agilent B1500A system that extracts polarization vs. voltage (P-V) and current vs. voltage (I-V) measurements based on varying recovery stress, stress voltage and frequency.

III. RESULTS AND DISCUSSION

A. MECHANISM STUDY OF RECOVERY EFFECT

Fig. 2 demonstrates the measurement sequences during the fatigue, recovery, and re-fatigue phases. To investigate current peak and its intensity, PUND pulses were applied as a

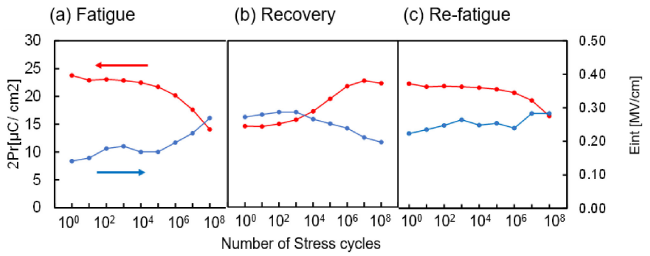

FIGURE 4. Remanent polarization and E_{in} as a function of cycling stress during (a) Fatigue, (b) Recovery, and (c) Re-fatigue phases. $2{\cdot}P_r$ was extracted by PUND pulse subscribing dielectric contribution in the left vertical axis. E_{int} was extracted by a formula of $1/2(|Ec_p|-|Ec_n|)$ in the right vertical axis. The coercive fields were extracted from the voltage with the peak current shown in the bottom I-V curves of in Fig. 3.

read sequence using voltages ranging from −2.8 V to 2.8 V, which is a higher range than the cycling stress during the fatigue phase to clearly identify a split current peak. The cycling stress conditions obtained corresponded to the condition shown in Fig. 1. Fig. 3 shows the P-V and I-V curves during the fatigue, recovery and re-fatigue phases. A current peak split at a cycling stress voltage of 2.0 V was observed during the fatigue and re-fatigue phases, indicating that some domains cannot be flipped because the fixed domains exhibit a higher coercive field. During the recovery phase, the split current peak first merged, and then the current peak intensity increased. A remanent polarization ($2{\cdot}P_r$) as a function of cycling stress during each phase in Fig. 2 was described in Fig. 4 using red lines. The $2{\cdot}P_r$ degradation and recovery were compatible with the ΔV_{BL} in Fig. 1. An internal field (E_{int}) was derived from (1).

$$E_{int} = \frac{1}{2}(|Ec_p| - |Ec_n|) \tag{1}$$

where Ec_p and Ec_n represent positive and negative coercive fields, respectively. The coercive fields were extracted from the voltage with the peak current shown in the bottom I-V curves of Fig. 3. A positive E_{int} was observed, implying that a more positively charged oxygen vacancies should exist on the surface of the bottom electrode than that at the surface of top electrodes. The E_{int} increased with cycling stress in the fatigue phase, whereas in the recovery phase it decreased, which supports the fact that a positively charged oxygen vacancy generated by electron de-trapping at bottom electrodes could cause domain pinning during the fatigue phase and can be neutralized in the recovery phase. Reference [19] The E_{int} is represented by the blue lines shown in Fig. 4.

From the result of current peak splitting behavior and decrement of E_{int}, the recovery mechanism can be explained as shown in Fig. 5. In the initial state, there could be pinned domains that were not flipped by a stress voltage during the fatigued phase (Fig. 5(a)), with a higher coercive field. When a higher cycling stress was applied to the fatigued capacitor, the pinned domain started to flip via neutralization of the positively charged oxygen vacancy accompanied by electron de-trapping at the interfacial layer (Fig. 5(b)) resulting in

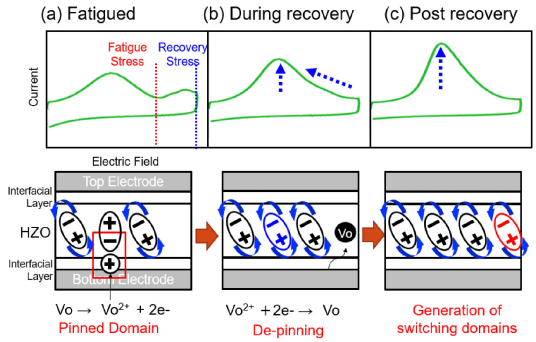

FIGURE 5. Recovery model during (a) Fatigue, (b) Recovery, and (c) Further-recovery phases. I-V image extracted from Positive pulse in PUND sequence at upper row. Image of switching behavior of domains at bottom row.

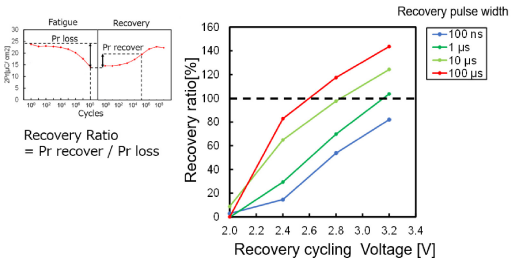

FIGURE 6. Recovery ratio calculation as a function of recovery cycling voltage ranging from 2.0 V to 3.2 V (step 0.4 V) with different pulse width of 100 ns, 1 µs, 10 µs and 100 µs. Definition of the recovery ratio was described by left graph.

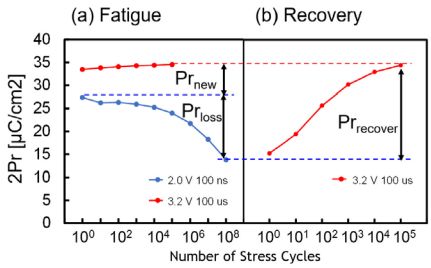

FIGURE 7. 2·Pr as a function of the cycling number during (a) fatigue with different conditions, i.e., 3.2 V with 100 µs in red and 2.0 V with 100 ns in blue. (b) Recovery at 3.2 V with 100 µs.

merged current peak splits. As the recovery cycling stress increases, oxygen vacancies are redistributed owing to factors similar to those observed during wake-up behavior, such as phase change [21] or reorientation of domains (in-plane to out-of-plane) [22], resulting in more switching domains that can participate in remanent polarization (Fig. 5. (c)). The gradual sharpening of the peak could be due to the migration of oxygen vacancies to the grain boundary during recovery stress. Reference [23] In addition to including the recovered domains that were fixed during fatigue, the switching domains also include wake-up domains that did not work under fatigued stress from the beginning. If further recovery stress cycles are applied, domain pinning or dielectric breakdown may occur owing to the stronger stress.

B. QUALIFICATION OF RECOVERY EFFECT

A recovery effect was qualified by investigating various recovery stress pulses. Different recovery voltages and pulse widths shown in Fig. 2(b) were applied post fatigue stress shown in Fig. 2(a). Fig. 6 shows a qualification of the recovery effect obtained from the recovery voltage and pulse width dependence. The recovery ratio was determined by (2),

$$Recovery\ ratio = P_{r\_recover}/P_{r\_loss} \tag{2}$$

where P_{r_loss} is the remanent polarization degradation post 10^8 cycles with a cycling stress voltage of 2.0 V, and $P_{r\_recover}$ is the amount of P_r recovered from the fatigue post 10^5 recovery cycles. Higher recovery ratio was obtained with higher cycling voltage and longer pulse width. There was no recovery effect observed at 2.0 V, and this was similar to that observed for fatigued stress voltage including when the pulse width was longer. Moreover, a large recovery ratio was obtained at recovery stresses higher than 2.4 V, indicating that a higher recovery voltage was required for the recovery phase, contrary to a higher fatigue stress voltage. Furthermore, the recovery ratio increased above 100% when the recovery stresses and pulse widths where 2.8 V, 3.2 V, 100 µs, and 10 µs, respectively. The impact of new wake-up domains caused by the recovery stress is investigated in Fig. 7. The 2·Pr of the recovery stage under the condition of 3.2 V with 100 µs was saturated to the value of the fatigue stage under the same condition of the fatigue phase. This indicates that domains, which were not involved in switching during fatigue (Pr_{new}), contribute to increase the recovery rate above 100% as illustrated in Fig. 5(c). The recovery cycling voltage dependence of the switching current with a fixed pulse width of 1 µs is shown in Fig. 8. It can be observed that when the recovery stress voltage was 2.4 V, the current peak split was unmerged, and the current peak intensity was saturated, indicating that the current peak split should be suppressed first by applying a higher recovery stress voltage. Fig. 9 shows the recovery cycling pulse width dependence of the switching current with a fixed stress voltage of 3.2 V. The current peak split was merged including when the pulse width was 100 ns, and a higher current peak was obtained post 10^5 cycles with a longer recovery pulse width. These results summarized that the domain depinning and generation of polar domains can occur simultaneously under higher recovery voltage or longer recovery pulse conditions.

IV. CONCLUSION

In this study, we have extended prior work and performed a detailed analysis using a single large capacitor that was fabricated using the same process as 1T1C FeRAM to clearly understand the recovery mechanism of memory windows and qualify the recovery effect. First, a peak splitting behavior and its intensity were monitored during the fatigue, recovery, and re-fatigue phases. The E_{int} increased with cycling stress during the fatigue phase and decreased during the recovery

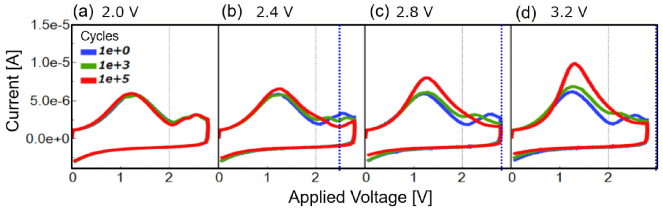

FIGURE 8. **I-V curve during recovery cycling post fatigue stress with a different voltage condition of (a) 2.0 V, (b) 2.4 V, (c) 2.8 V, and (d) 3.2 V, respectively. Pulse widths were fixed as 1 μs among these conditions. Only positive pulse during PUND pulse subscribing was described for simplicity.**

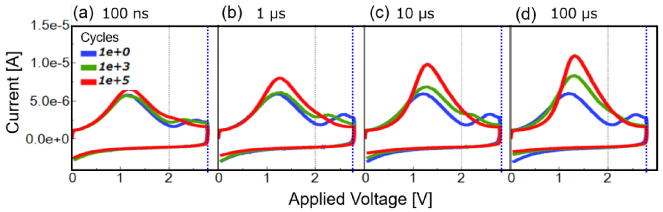

FIGURE 9. **I-V curve during recovery cycling post fatigue stress with a pulse width condition of (a) 100 ns, (b) 1 μs, (c) 10 μs, and (d) 100 μs, respectively. Voltage of the pulses were fixed as 3.2 V among these conditions. Only positive pulse during PUND pulse subscribing was described for simplicity.**

phase. During the recovery phase, the current peak splits first merged, and then the current peak intensity increased. These results suggest a recovery mechanism in which positively charged oxygen vacancies are neutralized, resulting in domain de-pinning, followed by redistributed oxygen vacancies forming new switching domains. The recovery effect was qualified by investigating the recovery voltage and pulse width dependence of the recovery ratio. A recovery ratio above 100% was obtained at a higher recovery voltage and longer recovery pulse width, which is in good agreement with the mechanism that domain de-pinning and new domains contribute to remanent polarization increment. A higher recovery ratio was obtained at a higher recovery voltage or longer pulse width in contrast to the stress condition of the fatigue phase, and the recovery voltage can be reduced by applying longer recovery pulse widths. Therefore, this technology enables greater flexibility of 1T1C FeRAM circuit design in improving the cycling endurance.

REFERENCES

[1] T. S. Böscke, J. Müller, D. Bräuhaus, U. Schröder, and U. Böttger, "Ferroelectricity in hafnium oxide thin films," *Appl. Phys. Lett.*,vol. 99, no. 10, 2011, Art. no. 102903, doi: 10.1063/1.3634052.

[2] S. Dünkel et al., "A FeFET based super-low-power ultra-fast embedded NVM technology for 22nm FDSOI and beyond," in *Proc. IEEE Int. Electron Devices Meeting (IEDM)*, 2017, pp. 1–14, doi: 10.1109/IEDM.2017.8268425.

[3] S. Fujii et al., "First demonstration and performance improvement of ferroelectric HfO2-based resistive switch with low operation current," in *Proc. IEEE Symp. VLSI Technol.*, 2016, pp. 1–2, doi: 10.1109/VLSIT.2016.7573413.

[4] U. Schroeder, C. S. Hwang, and H. Funakubo, Eds., *Ferroelectricity in Doped Hafnium Oxide: Materials, Properties and Devices*. Duxford, U.K.: Woodhead Publ., 2019.

[5] U. Schroeder et al., "Impact of different dopants on the switching properties of ferroelectric hafniumoxide," *Jpn. J. Appl. Phys.*, vol. 53, no. 8S1, p. 8LE02, 2014, doi: 10.7567/JJAP.53.08LE02.

[6] J. Müller et al., "Ferroelectricity in simple binary ZrO_2 and HfO_2," *Nano Lett.*, vol. 12, no. 8, pp. 4318–4323, 2012, doi: 10.1021/nl302049k.

[7] A. Toriumi et al., "Material perspectives of HfO_2-based ferroelectric films for device applications," in *Proc. IEEE Int. Electron Devices Meeting (IEDM)*, 2019, pp. 1–4, doi: 10.1109/IEDM19573.2019.8993464.

[8] M. Materano, C. Richter, T. Mikolajick, and U. Schroeder, "$Hf_xZr_{1-x}O_2$ thin films for semiconductor applications: An Hf-and Zr-ALD precursor comparison," *J. Vac. Sci. Technol. A*, vol. 38, no. 2, Mar. 2020, Art. no. 22402, doi: 10.1116/1.5134135.

[9] T. Francois et al.,"Demonstration of BEOL-compatible ferroelectric Hf0.5Zr0.5O2 scaled FeRAM co-integrated with 130nm CMOS for embedded NVM applications," in *Proc. IEEE Int. Electron Devices Meeting (IEDM)*, 2019, pp. 1–4, doi: 10.1109/IEDM19573.2019.8993485.

[10] J. Okuno et al., "SoC compatible 1T1C FeRAM memory array based on ferroelectric $Hf_{0.5}Zr_{0.5}O_2$," in *Proc. IEEE Symp. VLSI Technol.*, 2020, pp. 1–2, doi: 10.1109/VLSITechnology18217.2020.9265063.

[11] J. Okuno et al., "1T1C FeRAM memory array based on ferroelectric HZO with capacitor under bitline," *IEEE J. Electron Devices Soc.*, vol. 10, pp. 29–34, 2022, doi: 10.1109/JEDS.2021.3129279.

[12] J. Okuno et al., "High-endurance and low-voltage operation of 1T1C FeRAM arrays for nonvolatile memory application," in *Proc. IEEE Int. Memory Workshop*, 2021, pp. 1–3, doi: 10.1109/IMW51353.2021.9439595.

[13] J. Okuno et al., "Reliability study of 1T1C FeRAM arrays with $Hf_{0.5}Zr_{0.5}O_2$, thickness scaling," *IEEE J. Electron Devices Soc.*, vol. 10, pp. 778–783, 2022, doi: 10.1109/JEDS.2022.3187101.

[14] E. Yurchuk et al., "Origin of the endurance degradation in the novel HfO2-based 1T ferroelectric non-volatile memories," in *Proc. IEEE Symp. VLSI Technol. Int. Rel. Phys. Symp. (IRPS)*, 2014, pp. 1–5, doi: 10.1109/IRPS.2014.6860603.

[15] M. Peric et al., "Root cause of degradation in novel HfO_2-based ferroelectric memories," in *Proc. IEEE Symp. VLSI Technol. IEEE Int. Rel. Phys. Symp. (IRPS)*, 2016, pp. 1–5, doi: 10.1109/IRPS.2016.7574619.

[16] N. Gong and T.-P. Ma, "A study of endurance issues in HfO_2-based ferroelectric field effect transistors: Charge trapping and trap generation," *IEEE Electron Device Lett.*, vol. 39, no. 1, pp. 15–18, Jan. 2018, doi: 10.1109/LED.2017.2776263.

[17] S. Starschich, T. Schenk, U. Schroeder, and U. Boettger, "Ferroelectric and piezoelectric properties of $Hf_{1-x}Zr_xO_2$ and pure ZrO2 films," *J. Appl. Phys. Lett.*, vol. 110, May 2017, Art. no. 182905, doi: 10.1063/1.4983031.

[18] P. J. Liao et al., "Characterization of fatigue and its recovery behavior in ferroelectric HfZrO," in *Proc. IEEE Symp. VLSI Technol.*, 2021, pp. 1–2.

[19] T. Gong et al., "$10^5\times$ endurance improvement of FE-HZO by an innovative rejuvenation method for 1z node NV-DRAM applications," in *Proc. IEEE Symp. VLSI Technol.*, 2021, pp. 1–2.

[20] J. Okuno et al., "Demonstration of fatigue and recovery phenomena in $Hf_{0.5}Zr_{0.5}O_2$-based 1T1C FeRAM memory arrays," in *Proc. 6th IEEE Electron Devices Technol. Manuf.*, 2022, pp. 64–66, doi: 10.1109/EDTM53872.2022.9797943.

[21] S. Fields et al., "Phase-exchange-driven wake-up and fatigue in ferroelectric hafnium zirconium oxide films," *ACS Appl. Mater. Interfaces*, vol. 12, no. 23, pp. 26577–26585, 2020, doi: 10.1021/acsami.0c03570.

[22] M. Lederer et al., "Structural and electrical comparison of Si and Zr doped hafnium oxide thin films and integrated FeFETs utilizing transmission Kikuchi diffraction," *Nanomaterials*, vol. 10, no. 2, p. 384, 2020, doi: 10.3390/nano10020384.

[23] R. Winkler et al., "Controlling the formation of conductive pathways in memristive devices," *Adv. Sci.*, vol. 9, no. 33, 2022, Art. no. 2201806, doi: 10.1002/advs.202201806.